Journal of Neuroinflammation

RESEARCH

Open Access

Interferon-gamma receptor signaling regulates innate immunity during *Staphylococcus aureus* craniotomy infection

Zachary Van Roy[1†], Gunjan Kak[1†], Rachel W. Fallet[1] and Tammy Kielian[1*]

Abstract

A craniotomy is a neurosurgical procedure performed to access the intracranial space. In 3–5% of cases, infections can develop, most caused by *Staphylococcus aureus* biofilm formation on the skull surface. Medical management of this infection is difficult, as biofilm properties confer immune and antimicrobial recalcitrance to the infection and necessitate additional surgical procedures. Furthermore, treatment failure rates can be appreciably high. These factors, compounded with rapidly expanding rates of antimicrobial resistance, highlight the need to develop alternative treatment strategies to target and reverse the immune dysfunction that occurs during biofilm infection. Our recent work has identified $CD4^+$ Th1 and Th17 cells as potent regulators of innate immune cell activation during craniotomy infection. Here, we report the role of IFN-γ, versus other Th1- and Th17-derived cytokines, in programing the immune response to biofilm infection using both global and cell type-specific IFN-γR1-deficient (*Ifngr1*$^{-/-}$) mice. Bacterial burdens were significantly higher in *Ifngr1*$^{-/-}$ relative to WT animals despite few changes in immune cell abundance. Single-cell transcriptomics identified candidate explanations for this phenotype as alterations in cell death pathways, innate immune cell activation, MHC-II expression, and T cell responses were significantly reduced in *Ifngr1*$^{-/-}$ mice. While caspase-1 activation in PMNs and macrophage/microglial MHC-II expression were regulated by IFN-γ signaling, no phenotypes were observed with either granulocyte- or macrophage/microglia *Ifngr1*$^{-/-}$ conditional knockout mice, suggestive of redundancy. Instead, a decreased Th1/Th17 ratio was identified in *Ifngr1*$^{-/-}$ animals that was corroborated by elevated IL-17 levels and correlated with dysfunctional T cell-innate immune communication. Further, Th17 cells were less effective than Th1 cells in promoting *S. aureus* bactericidal activity in microglia and macrophages. Collectively, this work identifies a key protective role for IFN-γ during craniotomy infection by enhancing macrophage and microglial antibacterial activity. Therefore, controlled programming of IFN-γ responses may represent a novel therapeutic strategy for chronic craniotomy infections.

Keywords IFN-γR, T cells, Th1, Th17, Craniotomy, Biofilm, Infection, Macrophage, Microglia, Granulocyte

†Zachary Van Roy and Gunjan Kak contributed equally to this work.

*Correspondence:
Tammy Kielian
tkielian@unmc.edu
[1]Department of Pathology, Microbiology, and Immunology, University of Nebraska Medical Center, Nebraska Medical Center, Omaha, Nebraska 68198, USA

Introduction

Craniotomy involves the temporary excision of a skull segment (bone flap) to access the intracranial compartment [1]. This procedure enables the excision of brain tumors, evacuation of hematomas, and the implantation of medical devices such as those used in the treatment of Parkinson's disease or epilepsy [1, 2]. As such, craniotomy ranks among the most common neurosurgical interventions. However, in 3–5% of cases, infection can complicate surgical recovery [2–7]. Half of craniotomy infections are caused by *Staphylococcus aureus* (*S. aureus*) [2], which forms a biofilm on the bone flap surface and evades antibiotic- and immune-mediated clearance [2, 8, 9]. Therefore, surgical tissue debridement complemented with long-term systemic antibiotics remains the sole treatment strategy available to patients, an approach increasingly threatened by mounting antibiotic resistance [10]. These points necessitate the development of alternative treatment strategies, such as those that augment immune function, to promote biofilm clearance. This would effectively circumvent the need for additional surgeries to reduce patient morbidity, mortality, and resource strain on the healthcare system [6].

Our laboratory has extensively characterized the immune response to craniotomy infection, both in patients [2] and a mouse model [8, 11–17] that displays high congruence to its clinical counterpart [2]. In both cases, a segregated pattern of leukocyte recruitment was identified [2, 9, 12]. Specifically, the subcutaneous galea (directly above the bone flap and beneath the scalp) primarily contains neutrophils (PMNs) and granulocytic myeloid-derived suppressor cells (G-MDSCs), an alternatively programmed granulocytic subset with anti-inflammatory properties [18–20]. During craniotomy infection, G-MDSC formation is likely induced by the infection microenvironment since they are absent from the blood [2, 21]. G-MDSCs are also found in numerous other pathologies [22–26] where their origins are less clear. In contrast to the galea, the infected brain parenchyma displays immunological diversity typified by monocytes, macrophages, NK cells, T cells, granulocyte subsets, and tissue-resident microglia [2, 9, 12]. Many of these cell types have been linked to bacterial clearance, as the numbers of activated microglia correlate with reduced bacterial titers in the brain [15] and TLR2 deficiency or depletion of either granulocytes or $CD4^+$ T cells in wild type (WT) mice significantly increased bacterial burdens in the brain, galea, and on the bone flap [11, 12, 27]. Regarding the latter, adoptive transfer experiments in $Rag1^{-/-}$ mice identified that both $CD4^+$ Th1 and Th17 cells were protective during craniotomy infection [27] and these subsets were enriched during human craniotomy infection [2]. Further, flow cytometry and transcriptomic analysis identified a strong IFN-γ signature in T cells and innate immune cells infiltrating the brain. Even Th0 and Th17 cells adoptively transferred into *Rag1*-deficient mice were driven towards robust IFN-γ production, suggesting a Th1 bias at the site of craniotomy infection [27]. However, the direct role of IFN-γ vs. other Th cytokines during infection remains to be determined. Here we address this question by delineating the functional importance of IFN-γ signaling during craniotomy infection using IFN-γR1-deficient ($Ifngr1^{-/-}$) mice. $Ifngr1^{-/-}$ animals displayed heightened bacterial burdens compared to WT mice without large alterations in immune cell recruitment. Single-cell transcriptomics revealed reduced IFN signaling, antigen presentation, and immune activation pathways across several $Ifngr1^{-/-}$ innate immune populations, in agreement with previously documented roles for IFN-γ signaling in other systems [28–42]. No changes in craniotomy infection were evident with granulocyte- or macrophage/microglia-specific $Ifngr1^{-/-}$ mice, suggesting redundancy in IFN-γ signaling across multiple innate immune populations. Instead, scRNA-seq and inflammatory mediator analysis identified heightened Th17 polarization in $Ifngr1^{-/-}$ mice, which was associated with less microglial and macrophage bactericidal activity compared to Th1 stimulation. This work implicates innate immune programming via IFN-γ signaling as a key mechanism for bacterial containment during craniotomy infection.

Materials and methods

Mice

$Ifngr1^{-/-}$ mice were obtained from The Jackson Laboratory (RRID: IMSR_JAX:0032880) with C57BL/6J mice (RRID: IMSR_JAX:000664) used as WT controls. $Ifngr1^{-/-}$ conditional animals ($Cx3cr1^{Cre}Ifngr1^{fl/fl}$ and $Mrp8^{Cre}Ifngr1^{fl/fl}$) were generously provided by Dr. Keer Sun and have been previously utilized for targeted deletion of IFN-γR1 in macrophages [43, 44]. These strains were originally generated by crossing $Ifngr1^{fl/fl}$ (RRID: IMSR_JAX:025394) mice with $Cx3cr1^{Cre}$ (RRID: IMSR_JAX:025524) or $Mrp8^{Cre}$ (RRID: IMSR_JAX:021614) strains, as previously described [43] with WT littermates ($Cx3cr1^{Null}Ifngr1^{fl/fl}$ and $Mrp8^{Null}Ifngr1^{fl/fl}$) as controls. $Cx3cr1^{Cre}Ifngr1^{fl/fl}$ mice were functionally validated using readouts related to IFN-γ signaling including nitric oxide (NO) production [45], MHC-II expression [46], and proinflammatory cytokine production [28]. Briefly, bone marrow-derived macrophages were generated from $Cx3cr1^{Cre}Ifngr1^{fl/fl}$ mice and WT littermates, as described below and treated with peptidoglycan (10 μg/mL) and/or IFN-γ (200 ng/mL) for 24 h. Levels of nitrite, a stable end product following the reaction of NO with O_2, were measured in conditioned medium using the Griess reagent as previously described [47]. MHC-II levels were assessed by flow cytometry as outlined below and cytokine (IL-12,

IL-6, and TNF) production was quantified in supernatants with a Mouse Inflammation Cytometric Bead Array (Cat. #552364, BD Biosciences) as previously described [17]. All animals were bred in-house in the University of Nebraska Medical Center (UNMC) vivarium, where they were group-housed under a 12 h light/dark cycle with controlled temperature (~22 °C) and humidity (30–70%) with free access to food (2019 S Teklad Global 19% Protein Extruded Rodent Diet; Inotiv, West Lafayette, IN) and water (Hydropac; Lab Products, Seaford, DE). Nestlets were provided for enrichment. The animal use protocol was approved by the UNMC Institutional Animal Care and Use Committee (IACUC; 16-123-10) and conforms to relevant standards as described in the Public Health Service (PHS) Policy on the Human Care and Use of Laboratory Animals, the Guide for the Care and Use of Laboratory Animals, and the UNMC IACUC Animal Welfare Assurance, Guidelines and Policies.

Mouse model of *S. aureus* craniotomy infection

Craniotomy infection was established in 8- to 10-week-old male and female mice as previously described [17]. Briefly, animals were anesthetized with ketamine/xylazine i.p., whereupon a midline incision was made in the scalp to expose the cranium. A high-speed pneumatic drill (Stryker Corporation, Kalamazoo, MI) was used to excise a segment of the skull (i.e., bone flap), which was incubated in 10^6 colony forming units (CFUs) of *S. aureus* [USA300 LAC13C [48]] diluted in brain-heart infusion broth at 37 °C for 5 min, washed in sterile PBS, and reimplanted to seal the cranium. The resulting infectious inoculum (10^3 CFU/bone flap) [17] accurately models the low bacterial exposure associated with surgical site infection in patients [49]. The incision was closed using 6 – 0 nylon suture (Henry Schein, Melville, NY), whereupon animals received extended-release buprenorphine for pain relief and supplemental heat until they emerged from anesthesia. This procedure is associated with a low mortality rate (< 1%), which mainly results from anesthesia-related complications. The model has been validated to generate robust biofilm formation on the bone flap surface [9], which exhibits hallmark recalcitrance to systemic antibiotic treatment [2, 8].

Tissue collection and quantification of bacterial and immune cell abundance

At the indicated post-surgical interval (days 7 or 14 post-infection), mice were euthanized via isoflurane overdose and perfused with sterile PBS. The bone flap was removed, placed in 0.5 mL of 10% FBS in PBS, vortexed for 30 s, and an aliquot was removed for immune cell quantification. The bone flap was then sonicated for 5 min to dislodge the adherent biofilm and saved for bacterial enumeration. The galea, representing the subcutaneous tissue below the scalp and above the infected bone flap, was harvested by dissecting forceps into 0.5 mL of 10% FBS in PBS, homogenized with the blunt end of a syringe plunger, filtered through a 70 µm filter, and saved for quantification of immune infiltrates. An aliquot of the galea was taken prior to filtering and used for bacterial enumeration. The brain hemisphere beneath the infected bone flap was collected and placed in 1.5 mL of 10% FBS in PBS. Brain tissue was dissociated through a 70 µm filter, where an aliquot was taken for bacterial enumeration before collagenase digestion and myelin removal. The resulting single cell suspension was used to quantify immune populations, as previously described [17]. In some experiments, the spleen, kidney, and liver were collected to assess *S. aureus* dissemination and processed as described for the galea. Bacterial abundance in each tissue was assessed by serial dilution on tryptic soy agar (TSA) plates with 5% sheep blood (Remel/Thermo Scientific, Lenexa, KS).

Samples retained for quantification of immune populations by flow cytometry were incubated in TruStain FcX (BioLegend, San Diego, CA) to limit non-specific antibody binding. The following antibody panel was utilized in these experiments: CD45-Brilliant Violet 711™ (RRID: AB_2564383), Ly6G-Spark UV™ (RRID: AB_2924466), Ly6C-FITC (RRID: AB_394628), CD11b-Alexa Fluor® 700 (RRID: AB_394628), F4/80-Brilliant Violet 510™ (RRID: AB_2562622), CX3CR1-Brilliant Violet 785™ (RRID: AB_2565938), MHC-II-PE/Dazzle™ 594 (RRID: AB_2565979), γδ TCR-PE (RRID: AB_313832), CD3-APC (RRID: AB_2561455), CD4-Brilliant Violet 650™ (RRID: AB_2783035), CD8-Pacific Blue™ (RRID: AB_493425), and IFN-γR1 (CD119)-BD OptiBuild™ BV605 (RRID: AB_2742716). Due to the lack of microglia and adaptive immune cells in the galea and on the bone flap [9, 12, 15], the panel was restricted to granulocyte and monocyte markers for these samples. Cell viability was assessed using a Zombie UV Fixable Viability Kit (BioLegend, Cat. #423108) and AccuCount beads (Spherotech, Lake Forest, IL; Cat. #ACBP-100-10; 8.0–12.9 µm) were added to each sample to enable reporting of absolute cell counts. Samples were fixed with 1% paraformaldehyde (PFA) in PBS and acquisition was completed on a BD LSR Fortessa X50 cytometer with analysis using FlowJo (RRID: SCR_008520) and the gating strategies in Additional File 1: Fig. S1.

Quantification of inflammatory mediators

Inflammatory mediator expression in brain and galea homogenates was quantified using a MILLIPLEX MAP Mouse Cytokine/Chemokine Magnetic Bead Panel (Cat. #HT17MG-14 K-PX25, Millipore Sigma, Burlington, MA). Prior to use, homogenates were centrifuged at 14,000 rpm for 10 min at 4 °C to remove cell debris.

The assay was performed according to the manufacturer's instructions using a MAGPIX® xMAP instrument (Luminex, Austin, TX). Belysa® Analyst software (Millipore Sigma) was used to generate standard curves and interpolate experimental data. All values were standardized to sample protein content as assessed by bicinchoninic acid (BCA) assay.

Preparation of primary immune cells

Macrophages and PMNs were derived from the bone marrow of 8- to 12-week-old male and female mice as previously described [16, 17]. Briefly, bone marrow was extracted from the leg bones prior to red blood cell (RBC) lysis with water and rapid correction to isotonic conditions. Following RBC lysis, cells were cultured in RPMI-1640 with 10% FBS, penicillin/streptomycin/fungizone, 2 mM L-glutamine, 1% HEPES, 0.01% β-mercaptoethanol, and 10% conditioned medium from L929 fibroblasts as a source of macrophage colony-stimulating factor (M-CSF). Macrophage cultures were maintained at 37 °C with 5% CO_2 for 7 days with medium replacement on days 3 and 5. PMNs were isolated on the day of experiments from the bone marrow using Ly6G magnetic beads (Cat. # 130-120-337, Miltenyi Biotec, Gaithersburg, MD).

Primary microglia were prepared from 2- to 4-day-old mice as previously described [17]. Pups were euthanized by isoflurane overdose prior to isolating the cerebral cortex that was diced using sterile surgical scissors in cold PBS. Resulting brain tissue was digested in 0.5% trypsin-EDTA for 20 min at 37 °C, disrupted by repetitive pipetting, filtered, and cultured in 75-cm^2 flasks in a final volume of 20 mL of culture medium [DMEM + 10% FBS supplemented with penicillin/streptomycin/fungizone, OPI (oxalacetic acid, pyruvate, insulin; Millipore-Sigma, Burlington, MA), and 0.5 ng/mL recombinant mouse GM-CSF (BioLegend)]. Cells were maintained at 37 °C with 5% CO_2 for 6 days, with medium replacement on day 4, whereupon cells were trypsinized and transferred to 175-cm^2 flasks. Cultures were supplemented with additional medium (10 mL) on days 9 and 11 and harvested at confluence via light agitation to detach microglia from the astrocyte monolayer.

Naïve $CD4^+$ T cells were isolated from the spleens of 6- to 8-week-old mice. Spleens were homogenized and filtered through 70 µm nylon mesh before isolation using a MojoSort mouse naïve T cell isolation kit (Cat. #480040, BioLegend). T cells were cultured in RPMI supplemented with 10% FBS, penicillin/streptomycin/fungizone, 2 mM L-glutamine, 1% HEPES, and 0.01% β-mercaptoethanol. Th17 differentiation was achieved by seeding naïve T cells in a 96-well flat bottom plate coated with anti-CD3ε (RRID: AB_11149115) and anti-CD28 (RRID: AB_11147170). Cells were then treated with 30 ng/mL IL-6 (Cat. #575706, BioLegend), 10 ng/mL IL-23 (Cat. #589004, BioLegend), 10 ng/mL IL-1β (Cat. #575104, BioLegend) and 2 ng/mL TGF-β1 (Cat. #781804, BioLegend) along with 10 µg/mL each of anti-IFN-γ (RRID: AB_1089144), anti-IL-4 (RRID: AB_315316), and anti-IL-2 (RRID: AB_315292) for 3 days. Th1 polarization was achieved by exposure to anti-CD3ε/anti-CD28 mouse T-activator Dynabeads (Cat. #11456D, Thermo Fisher, Waltham, MA) at a 1:1 bead-cell ratio in combination with 10 µg/mL anti-IL-4 (RRID: AB_315316), 10 ng/mL IL-2 (Cat. #575406, BioLegend), and 10 ng/mL IL-12 (Cat. #577004, BioLegend) for 3 days. This approach has been previously validated in our laboratory to produce > 70% polarization efficiency for each Th cell subset [27].

Assessment of caspase-1 activation, apoptosis, and bactericidal capacity

Caspase-1 activity and apoptosis were assessed in PMNs in vitro using flow cytometry-based assays. Briefly, PMNs were recovered from the bone marrow as described above and treated with 200 ng/mL IFN-γ or vehicle for 1 h prior to stimulation with live *S. aureus* at a multiplicity of infection (MOI) of 10:1 (bacteria: PMN) for an additional hour. IFN-γ was maintained throughout the 2 h treatment period. Caspase-1 activity was quantified in PMNs using a Pyroptosis/Caspase-1 Assay (FLICA; Cat. #9158, Antibodies Incorporated, Davis, CA) and apoptosis with Apotracker™ Green (Cat. #427402, BioLegend) during a 1 h incubation in 2% FBS in PBS, followed by surface marker staining with Ly6G-PE (RRID: AB_1186099) and a Zombie UV Fixable Viability Kit (Cat. #423108, BioLegend). Caspase-1 activity was quantified in cells recovered from craniotomy infection tissues as described above; however, the following antibodies were used along with a Zombie UV Fixable Viability Kit (Cat. #423108, BioLegend) to avoid spectral overlap with the FLICA dye: Ly6G-Spark UV™ (RRID: AB_2924466), F4/80-Brilliant Violet 510™ (RRID: AB_2562622), CD11b-FITC (RRID: AB_312789), CD45-Pacific Blue™ (RRID: AB_493535), and Ly6C-PerCP-Cy5.5 (RRID: AB_1727558). Both assays were analyzed on a BD LSR-IIG cytometer.

The bactericidal capacity of macrophages and microglia co-cultured with Th1 or Th17 polarized cells was assessed by gentamicin protection assays as previously reported [17]. Briefly, microglia, macrophages, and Th cell subsets were prepared as described above. Microglia and macrophages were treated with live *S. aureus* at a MOI of 10:1 (bacteria: cell) for 1 h, whereupon remaining extracellular bacteria were killed by high-dose gentamicin (100 µg/mL) for 30 min, followed by a maintenance dose (1 µg/mL) to prevent bacterial outgrowth. Where indicated, microglia and macrophages were co-cultured with Th1 or Th17 cells at a 1:1 ratio and, at the indicated time points, cells were lysed with sterile water for 15 min,

serially diluted, and plated on blood agar plates to quantify intracellular bacterial abundance. For determining intracellular bacterial burdens in vivo, Ly6G$^+$ granulocytes and F4/80$^+$ microglia/macrophages were isolated from galea and brain homogenates, respectively, using magnetic beads (Cat. # 130-120-337 and 130-110-443, Miltenyi Biotec) prior to gentamicin treatment, water lysis, and bacterial enumeration as described above.

scRNA-seq

Single-cell suspensions were prepared from the brain and galea of WT and *Ifngr1*$^{-/-}$ mice at day 14 post-infection as described above and pooled (10 mice per sample). Samples were FACS-purified to obtain live CD45$^+$ cells and subjected to single-cell transcriptomics as previously described [2, 50, 51]. Briefly, samples were evaluated using a Luna automated fluorescent cell counter (Logos Biosystems) to assess cell viability, density, and debris before single-cell capture with a 10X Genomics instrument. Samples were freshly analyzed on the day of isolation with no exceptions. Cells were lysed, and the resulting RNA was reverse-transcribed and barcoded using a Chromium Single Cell 3′ Reagent Kit (v3.1; 10X Genomics, Pleasanton, CA) according to the manufacturer's instructions. Illumina-compatible cDNA libraries were quantified with a Qubit-30 Fluorometer and assessed using a fragment analyzer before loading on a Novaseq6000 instrument at a final concentration of 300 pM for generation of 75 bp pair-end reads. Samples sequenced included: WT brain (7,229 cells), WT galea (6,889 cells), *Ifngr1*$^{-/-}$ brain (6,732 cells), and *Ifngr1*$^{-/-}$ galea (6,776 cells). Sequencing was performed to an average depth of 50,000–100,000 reads per cell and datasets were deposited in the Gene Expression Omnibus (GEO) database (GSE282637).

Bioinformatics

Sequencing data was aligned to the mouse genome using 10X Genomics Cell Ranger (RRID: SCR_017344) and low-quality cells/reads were filtered out of the dataset using the Cell Ranger cell-calling algorithm [52] with an input specification of 5,000–10,000 cells. Due to the low multiplet rate reported for this technology (0.8–3.2%, 10X Chromium Single Cell 3′ Reagent Kit v3.1), doublet exclusion was not performed. scRNA-seq quality control metrics were examined in Cell Ranger and were consistent with high-quality data across all sequenced samples (Additional File 2). No further cell filtering was performed. The data was then imported into Partek Flow Genomics Suite (RRID: SCR_011860) for additional analysis similar to previously described [2]. Resulting single-cell count matrices were normalized in Partek Flow using counts per million, add 1, and log base 2 transformed. Cell type identification was performed as described previously [2] using the code in Additional File 3. Clustering was performed using the top 20 principal components and differential gene expression between each cluster was assessed using a Hurdle statistical model. Differential expression results were exported and further analyzed using IPA (RRID: SCR_008653). Identification of G-MDSC-like clusters was performed as outlined previously [2] using a published set of mouse G-MDSC specific genes [53]. Cellular communication networks were predicted using the CellChat v2 package [54] in R according to the manuals and tutorials presented by the creators of this tool [https://github.com/jinworks/CellChat]. The code used for this analysis is provided in Additional File 4.

Statistics

Significant differences between groups for immune populations, inflammatory mediator expression, or other assays were determined using either an unpaired two-tailed Student *t*-test, multiple unpaired *t*-test, two-way ANOVA with Šidák multiple comparisons test, chi-square test, or one sample Wilcoxon signed rank test, as appropriate, in GraphPad Prism (RRID: SCR_002798). Outliers were removed only for Milliplex assays using the ROUT method [55] (with Q = 1%; 0–3 observations per condition) in GraphPad Prism. A p-value of < 0.05 was used to reflect statistical significance. For sequencing analyses, significant differences were determined using an FDR-adjusted p-value of < 0.05. Figures were created in Partek Flow, GraphPad Prism, or BioRender.

Results

IFN-γR1 signaling is beneficial during craniotomy infection

Our previous work demonstrated that CD4$^+$ Th1 and Th17 cells are critical for bacterial containment during craniotomy infection [27]; however, both populations produce TNF as well as proinflammatory mediators unique to Th1 (IFN-γ and IL-2) and Th17 cells (IL-17, IL-21, and IL-22) [56–58] that could impact infectious outcomes. To isolate the role of IFN-γ, craniotomy infection was evaluated in *Ifngr1*$^{-/-}$ mice at days 7 and 14 post-infection, corresponding to time points of maximal T cell infiltration in the brain [15]. IFN-γR1 deficiency significantly worsened bacterial burden in the brain at both intervals, which extended to the galea at day 14 post-infection (Fig. 1A). No evidence of *S. aureus* dissemination to peripheral organs was observed in either WT or *Ifngr1*$^{-/-}$ mice (Additional File 1: Fig. S2A). IFN-γ is known to promote bactericidal activity [28, 45, 59, 60] and *S. aureus* can survive and proliferate intracellularly in macrophages and granulocytes [61, 62]. Intracellular bacterial burdens were significantly increased in both Ly6G$^+$ granulocytes and F4/80$^+$ microglia/macrophages recovered from *Ifngr1*$^{-/-}$ mice at day 14 post-infection

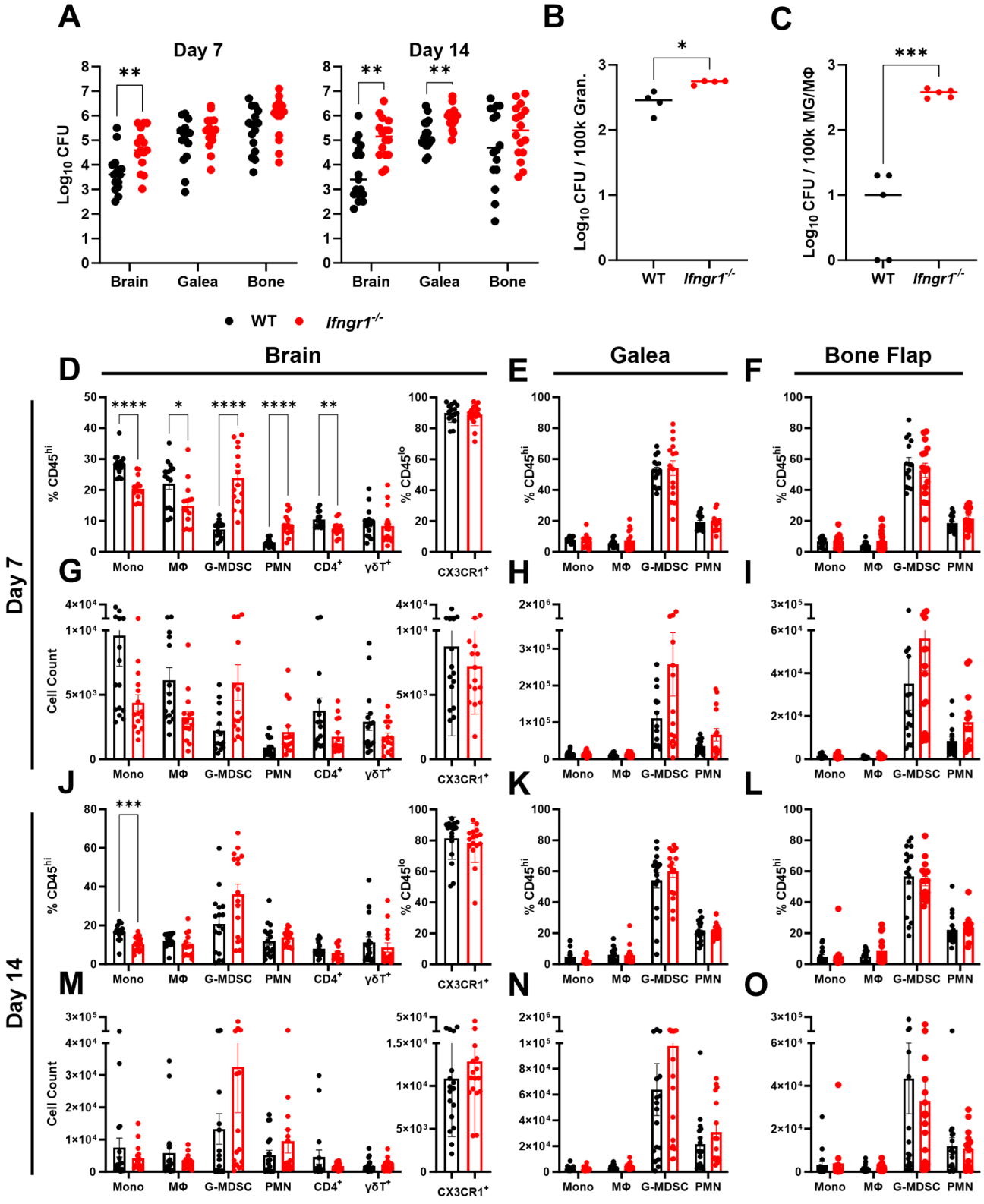

Fig. 1 IFN-γR1 signaling prevents *S. aureus* outgrowth during craniotomy infection. *Ifngr1*$^{-/-}$ ($n = 16$) and WT ($n = 15$–17) mice were subjected to craniotomy infection and sacrificed at days 7 and 14 post-infection, where (**A**) bacterial burdens and immune cell (**D-F**, **J-L**) percentages and (**G-I**, **M-O**) absolute counts were quantified from the brain, galea, and bone flap. Data pooled from three independent experiments (mean ± SEM) and analyzed by multiple unpaired *t*-test. (**B-C**) Intracellular bacterial burden in (**B**) Ly6G$^+$ granulocytes from the galea and (**C**) F4/80$^+$ microglia/macrophages from the brains of WT and *Ifngr1*$^{-/-}$ mice was assessed at day 14 post-infection using gentamicin protection assays. Data are from one experiment (mean ± SD) and analyzed by two-tailed Student's t-test. Mono, monocyte; MΦ, macrophage; MG, microglia; Bone, bone flap; *, $p < 0.05$; **, $p < 0.01$; ***, $p < 0.001$; ****, $p < 0.0001$

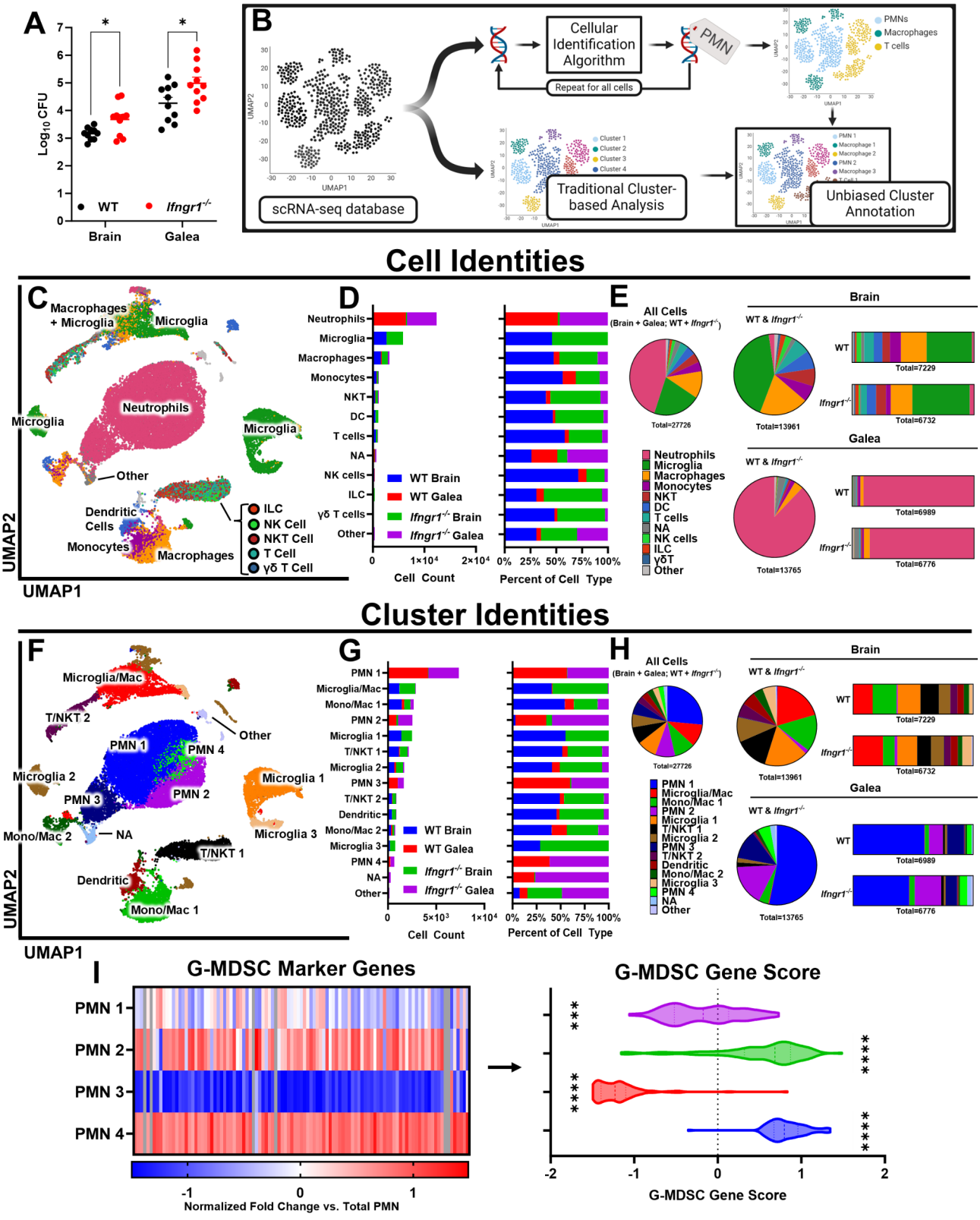

Fig. 2 (See legend on next page.)

(See figure on previous page.)

Fig. 2 Overview of single-cell transcriptomics dataset. CD45$^+$ cells were recovered from the brain and galea of WT and *Ifngr1*$^{-/-}$ animals at day 14 post-infection for scRNA-seq analysis (27,726 total cells). (**A**) Bacterial burden in mice ($n = 10$/strain) that were pooled for scRNA-seq. (**B**) Schematic of the cell and cluster annotation pipelines created with BioRender (https://BioRender.com/v90v103). For (**C-E**) cellular identities and (**F-H**) clusters, UMAP visualization is shown (**C**, **F**). This data is also presented as absolute and relative counts by sample (**D-E**, **G-H**). (**I**) G-MDSC cluster identity was determined using transcriptional expression of marker genes. Data analyzed by (**A**) multiple unpaired *t*-test or (**I**) one sample Wilcoxon signed rank test; *, $p < 0.05$; ***, $p < 0.001$; ****, $p < 0.0001$. DC, dendritic cell; ILC, innate lymphoid cell; Mono, monocyte; Mac, macrophage

compared to WT animals (Fig. 1B-C), which may account for heightened bacterial abundance in *Ifngr1*$^{-/-}$ tissues at this interval (Fig. 1A). Monocyte, macrophage, and CD4$^+$ T cell infiltrates were significantly decreased in brains of *Ifngr1*$^{-/-}$ mice at day 7 post-infection, whereas granulocytes (PMNs and G-MDSCs) were increased, which was attributed to elevated bacterial burdens in the brain at day 7 (Fig. 1D). Immune populations in the galea and bone flap were not altered by IFN-γR1 deficiency (Fig. 1E-F). Absolute cell counts followed similar trends but failed to reach significance due to variability between individual animals (Fig. 1G-I). Interestingly, these initial differences in immune infiltrates largely dissipated by day 14 post-infection (Fig. 1J-O) despite exaggerated bacterial burdens in the brain and galea of *Ifngr1*$^{-/-}$ mice at this time point (Fig. 1A). These data demonstrate that IFN-γR1 signaling is critical for bacterial containment during craniotomy infection, which is likely influenced by effects on immune cell activation since minimal changes were observed in cellular abundance.

Single-cell transcriptomics identifies immune dysfunction during IFN-γR1 deficiency

The lack of clear and persistent changes in immune cell abundance despite continued increases in bacterial burden in *Ifngr1*$^{-/-}$ mice (Fig. 1) suggests that IFN-γR1 deficiency results in functional immune cell deficits. To assess this possibility, scRNA-seq was performed on CD45$^+$ cells recovered from the brain and galea of WT and *Ifngr1*$^{-/-}$ mice at day 14 post-infection, representing the time point of most severe bacterial outgrowth (Fig. 1A). This approach was used based on the pleiotropic effects of IFN-γ on multiple immune cell populations [28–42], which can be captured by the scRNA-seq platform. We first confirmed that bacterial burdens were elevated in *Ifngr1*$^{-/-}$ brain and galea samples used for sequencing (Fig. 2A), aligning with our previous results (Fig. 1A). Following dataset normalization and uniform manifold approximation and projection (UMAP) visualization (Additional File 1: Fig. S2B), two parallel analyses were conducted to ensure unbiased annotation of cell types (Fig. 2B). This approach has been recommended in the literature for annotating cells into biologically meaningful groups [63] and yielded robust results in previous work [2, 15].

First, each cell was individually assigned a '*cell identity*' using previously-published custom code [2] and the SingleR package [64] with The Immunological Genome Project [65] as a reference database (Additional File 3). This step is cluster-independent and performed iteratively for each cell in the dataset, yielding broad cellular identities such as 'Neutrophil', 'Microglia', and 'Macrophage' (Fig. 2C). Neutrophils were identified as the most abundant cell type captured (Fig. 2D), comprising 44% of all 27,726 transcriptomes in our dataset and 88% from the galea (Fig. 2E), validating our flow cytometry findings (Fig. 1J-O). In agreement with our previous reports of a segregated immune response between the brain and galea [9, 12] (Fig. 1J-O), monocytes, macrophages, microglia, NK/NKT, and T cells were primarily detected in the brain, with few granulocytic infiltrates in this compartment (Fig. 2D-E). Importantly, cellular frequencies were similar between WT and *Ifngr1*$^{-/-}$ mice in both the brain and galea (Fig. 2D-E), agreeing with our flow cytometry data at day 14 post-infection (Fig. 1J-O).

Separately, the SLM algorithm [66] was used to identify 15 unique cell clusters in our dataset, representing groups of cells with similar transcriptional profiles (Fig. 2F). This analysis was rectified (Fig. 2B) with bioinformatically-determined cell identities (Fig. 2C-E) to accurately annotate cluster identities (Additional File 1: Fig. S2C), which will be used throughout this work. In this way, we identified 4 unique PMN, 3 microglial, 3 mixed monocytic, and 2 T/NKT clusters (Fig. 2F). The overall abundances of these clusters (Fig. 2G-H) largely recapitulated the cell identity analyses (Fig. 2D-E) but revealed additional heterogeneity within cell types. Importantly, cluster abundances in the brain and galea were roughly equivalent between WT and *Ifngr1*$^{-/-}$ mice (Fig. 2G-H; Additional File 1: Fig. S2B), enabling robust statistical comparisons. Of note, The Immunological Genome Project database [65] lacks the resolution to differentiate between PMNs and G-MDSCs based on their similarities [2, 67]. Therefore, identification of G-MDSC clusters was performed using a previously published G-MDSC gene score pipeline [2] and mouse G-MDSC marker genes [53], which identified PMN2 and PMN4 to be G-MDSC-like, with PMN1 and PMN3 classified as mature PMNs (Fig. 2I).

To identify alterations in cellular programming following IFN-γR1 loss, the top 8 clusters by cell count were subjected to differential analysis using a Hurdle/MAST model [68] where the transcriptomes of *Ifngr1*$^{-/-}$ cells were compared to WT within each cluster. This data was then exported and analyzed in parallel by both gene set

enrichment analysis (GSEA) [69] and Ingenuity Pathway Analysis (IPA) [70] to reveal significantly altered pathways which may explain the inability of *Ifngr1*$^{-/-}$ mice to control *S. aureus* growth (Fig. 1A). This approach identified broad transcriptional changes across most clusters with good concordance between GSEA and IPA (Fig. 3A-B). *Ifngr1*$^{-/-}$ led to global reductions in antigen presentation, interferon response, and immune activation/signaling pathways across multiple cell types, in particular related to T cell activation (Fig. 3A-B) aligning with the literature regarding IFN-γ effects [29–39, 41, 42]. Interestingly, IPA also revealed a granulocyte-specific reduction in pyroptosis pathways with IFN-γR1 deficiency (Fig. 3B). Transcriptional and cellular stress pathways were upregulated across *Ifngr1*$^{-/-}$ clusters (Fig. 3A-B), which may result from heightened bacterial burden in these samples eliciting an integrated stress response (ISR) [71] (Fig. 2A). Changes in MHC-II expression were validated by flow cytometry, which confirmed decreased MHC-II levels in *Ifngr1*$^{-/-}$ microglia as well as monocytes and macrophages relative to WT primarily in the brain (Additional File 1: Fig. S3A). Small but significant decreases in granulocyte MHC-II levels were also observed but were deemed biologically insignificant due to low MHC-II expression at baseline. MHC-II rebounded to WT levels in most cells by day 14-post infection except for microglia where expression remained significantly lower (Additional File 1: Fig. S3A-B). Similar reductions in MHC-II were observed in *Cx3cr*^{Cre}*Ifngr1*$^{fl/fl}$ mice lacking IFN-γR1 only on macrophages and microglia, supporting direct regulation by IFN-γ and validating targeting specificity (Additional File 1: Fig. S3C). Similar experiments were not conducted in granulocyte-specific *Ifngr1*$^{-/-}$ mice (*Mrp8*^{Cre}*Ifngr1*$^{fl/fl}$) due to low MHC-II levels in this population (Additional File 1: Fig. S3A-B). Collectively, these experiments identified multiple processes that may contribute to the exacerbated bacterial burden seen in *Ifngr1*$^{-/-}$ mice, including: [1] altered granulocyte pyroptosis and/or activation, [2] altered macrophage/microglial antigen presentation and/or activation, or [3] altered Th cell activation states. Each of these possibilities are addressed in the following sections.

IFN-γR1 signaling promotes caspase-1 activity in PMNs

Given our prior work demonstrating the importance of caspase-1 for bacterial containment during craniotomy infection [11] and transcriptional evidence of a granulocyte-specific defect in caspase-1-dependent pyroptosis

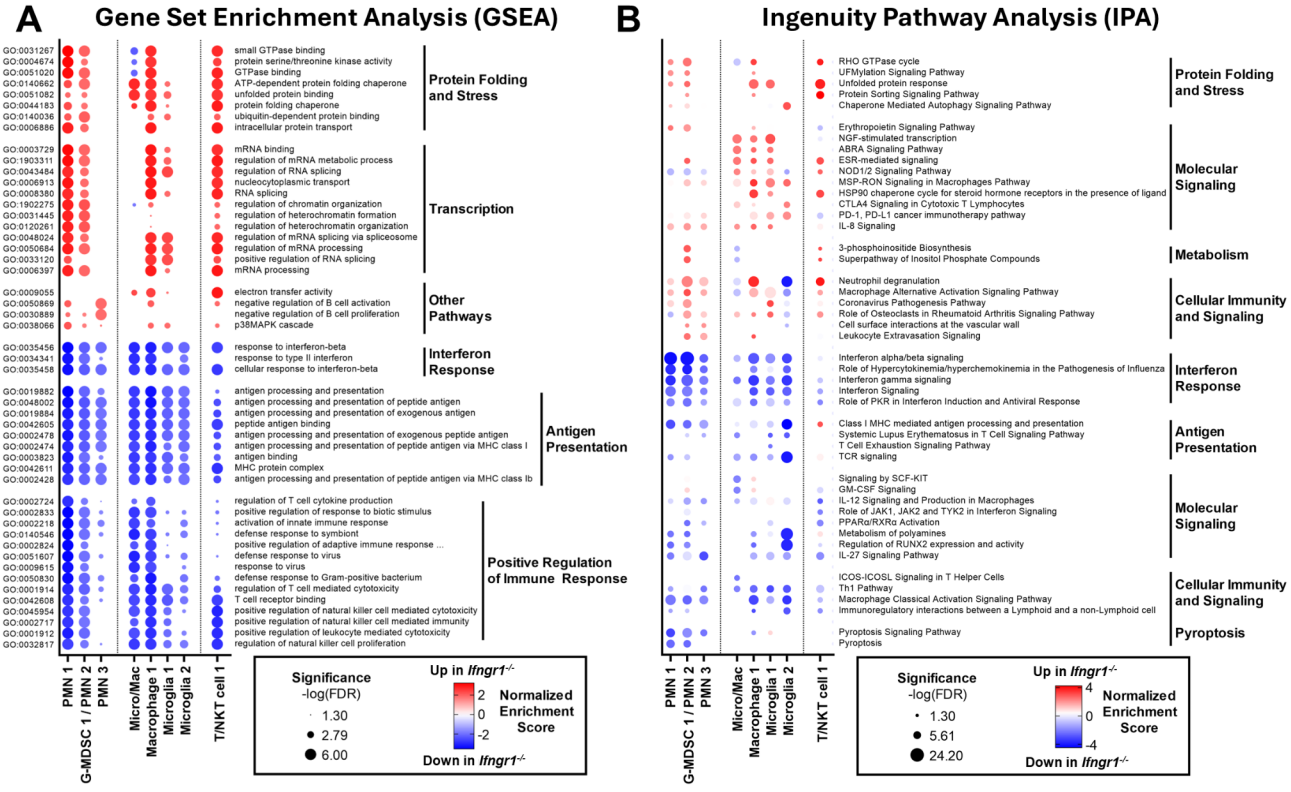

Fig. 3 Pathway analysis of differentially expressed genes between *Ifngr1*$^{-/-}$and WT mice during craniotomy infection. The scRNA-seq database derived from cells isolated from the brain and galea of *Ifngr1*$^{-/-}$ and WT mice ($n = 10$/strain) at day 14 post-infection was analyzed for transcriptional differences within clusters across strains. Differential gene expression was analyzed by (**A**) gene set enrichment analysis (GSEA) or (**B**) ingenuity pathway analysis (IPA) and is presented by cluster. A statistical pipeline in IPA was used to identify significant pathway differences, which relies on the right-tailed Fisher's Exact Test. Only significant results ($p < 0.05$) are denoted by colored circles; non-significant comparisons are omitted (white spaces)

in *Ifngr1*$^{-/-}$ mice (Fig. 3B), we explored whether altered granulocyte caspase-1 activity may contribute to worsened bacterial burden following IFN-γR1 loss. Indeed, pyroptosis-related genes, including *Stat1*, *Casp1*, and *Casp4* were markedly decreased in *Ifngr1*$^{-/-}$ cells relative to WT controls, particularly in granulocytic clusters (dashed circles; Fig. 4A). Treatment of PMNs with IFN-γ enhanced both apoptosis, as measured by cell surface phosphatidylserine staining (ApoTracker™), and caspase-1 activity (FLICA) in response to live *S. aureus* (Fig. 4B). As expected, IFN-γ had no effect on *Ifngr1*$^{-/-}$ PMNs. Interestingly, activated PMNs were largely double-positive for both assays (Fig. 4C). Since apoptosis and caspase-1-dependent pyroptosis are typically exclusive events [72] and phosphatidylserine residues have recently been linked to alternative forms of cell death besides apoptosis [73], it is possible that IFN-γ stimulation enhances pyroptosis in PMNs following exposure to live *S. aureus*.

While IFN-γ enhanced caspase-1 activity in PMNs during *S. aureus* exposure, bacteria alone were also capable of inducing caspase-1 (Fig. 4B-C). To determine whether IFN-γR1 signaling alters caspase-1 activity in vivo, levels were assessed in immune cells from WT and *Ifngr1*$^{-/-}$ mice at days 7 and 14 post-infection, which revealed no significant differences (Fig. 4D). Caspase-1 activity was highest in cells infiltrating the galea compared to the brain, in agreement with higher bacterial burdens in the former. Collectively, these findings suggest that while IFN-γR1 signaling can enhance PMN caspase-1 activity this is likely a minor response that is overshadowed by other inflammatory pathways, explaining the lack of a phenotype.

Beneficial effects of IFN-γR1 signaling during craniotomy infection cannot be attributed solely to macrophages/microglia or granulocytes

Since *Ifngr1*$^{-/-}$ mice displayed defects in *S. aureus* containment, we next examined whether this was attributable to a particular cell type(s) or instead required a broader response across multiple cell populations. IFN-γR1 levels were low on granulocytes (Fig. 4E), which correlated with a lack of alterations in bacterial burden or immune infiltrates in *Mrp8*^{Cre}*Ifngr1*$^{fl/fl}$ mice with granulocyte-specific deletion in IFN-γR1 (Additional File 1: Fig. S4A and C). Macrophages and microglia expressed higher levels of IFN-γR1 (Fig. 4E); however, IFN-γR1 deletion in these cell types (*Cx3cr1*^{Cre}*Ifngr1*$^{fl/fl}$) also had no effect on bacterial burden or immune populations, apart from a small but significant decrease in CD4$^+$ T cells (Additional File 1: Fig. S4B and D). IFN-γR1 targeting was confirmed in bone marrow-derived macrophages from *Cx3cr1*^{Cre}*Ifngr1*$^{fl/fl}$ mice, where NO production (Additional File 1: Fig. S5A), MHC-II expression (Additional File 1: Fig. S5B-C), and proinflammatory cytokine release (Additional File 1: Fig. S5D-F) were significantly decreased in response to peptidoglycan (PGN) and IFN-γ compared to macrophages from WT littermates. Collectively, these findings suggest the coordinated action of IFN-γR1 signaling across multiple innate immune cell types to prevent *S. aureus* outgrowth during craniotomy infection.

CD4$^+$ Th cell frequency is affected by IFN-γR1 deficiency during craniotomy infection

Given the limited phenotypes in *Cx3cr1*^{Cre}*Ifngr1*$^{fl/fl}$ and *Mrp8*^{Cre}*Ifngr1*$^{fl/fl}$ mice, we decided to take a broader approach and quantify inflammatory mediator expression in tissues from *Ifngr1*$^{-/-}$ animals to gain insights into potential mechanisms responsible for heightened bacterial burdens in these animals (Fig. 1A). IFN-γ levels were significantly elevated in *Ifngr1*$^{-/-}$ mice (Fig. 5A), which was attributed to the lack of a negative feedback loop resulting from IFN-γR1 loss. CXCL10 and CCL5 expression was significantly decreased in *Ifngr1*$^{-/-}$ mice relative to WT animals (Fig. 5C-D), in agreement with both being IFN-γ-induced chemokines [74, 75]. However, since leukocyte recruitment was unaffected in *Ifngr1*$^{-/-}$ mice (Fig. 1D-O) this was not likely responsible for elevated bacterial burdens in these animals. Strikingly, IL-17 was significantly increased in the brain and galea of *Ifngr1*$^{-/-}$ mice (Fig. 5B), suggesting elevated Th17 responses in the context of IFN-γR1 deficiency. This was further supported by increases in IL-1β and IL-6 in the brains of *Ifngr1*$^{-/-}$ mice (Additional File 1: Fig. S6), both of which are important for Th17 development [76]. Indeed, IFN-γ is known to inhibit Th17 formation to bias Th1 responses [41, 42], and IPA identified decreased Th1 signaling in numerous *Ifngr1*$^{-/-}$ populations relative to WT cells (Fig. 3B). Minimal changes were observed for other inflammatory mediators between *Ifngr1*$^{-/-}$ and WT mice (Additional File 1: Fig. S6).

To assess whether Th1/Th17 ratios were altered in *Ifngr1*$^{-/-}$ mice, we turned to our scRNA-seq dataset where the T/NKT1 and T/NKT2 clusters were bioinformatically segmented from the parent dataset (Fig. 5E), pooled, and re-clustered. This approach identified 7 unique T cell clusters (Fig. 5F) which were annotated based on marker gene expression as Th1, Th17, Treg, γδ T cell, and 'other' which lacked a dominant cell type (Additional File 1: Fig. S7A). Chi-square analysis confirmed altered proportions of T cells between *Ifngr1*$^{-/-}$ and WT mice (Fig. 5G), which was driven by decreased cell counts in the two Th1 clusters and increased Th17 and γδ T cell abundance (Fig. 5G **and H**). Treg and the 'other' clusters were similar between strains. These trends were also visually apparent in the UMAP space (Additional File 1: Fig. S7B). Collectively, these data suggest that IFN-γR1 deficiency enhances Th17 and γδ T cell

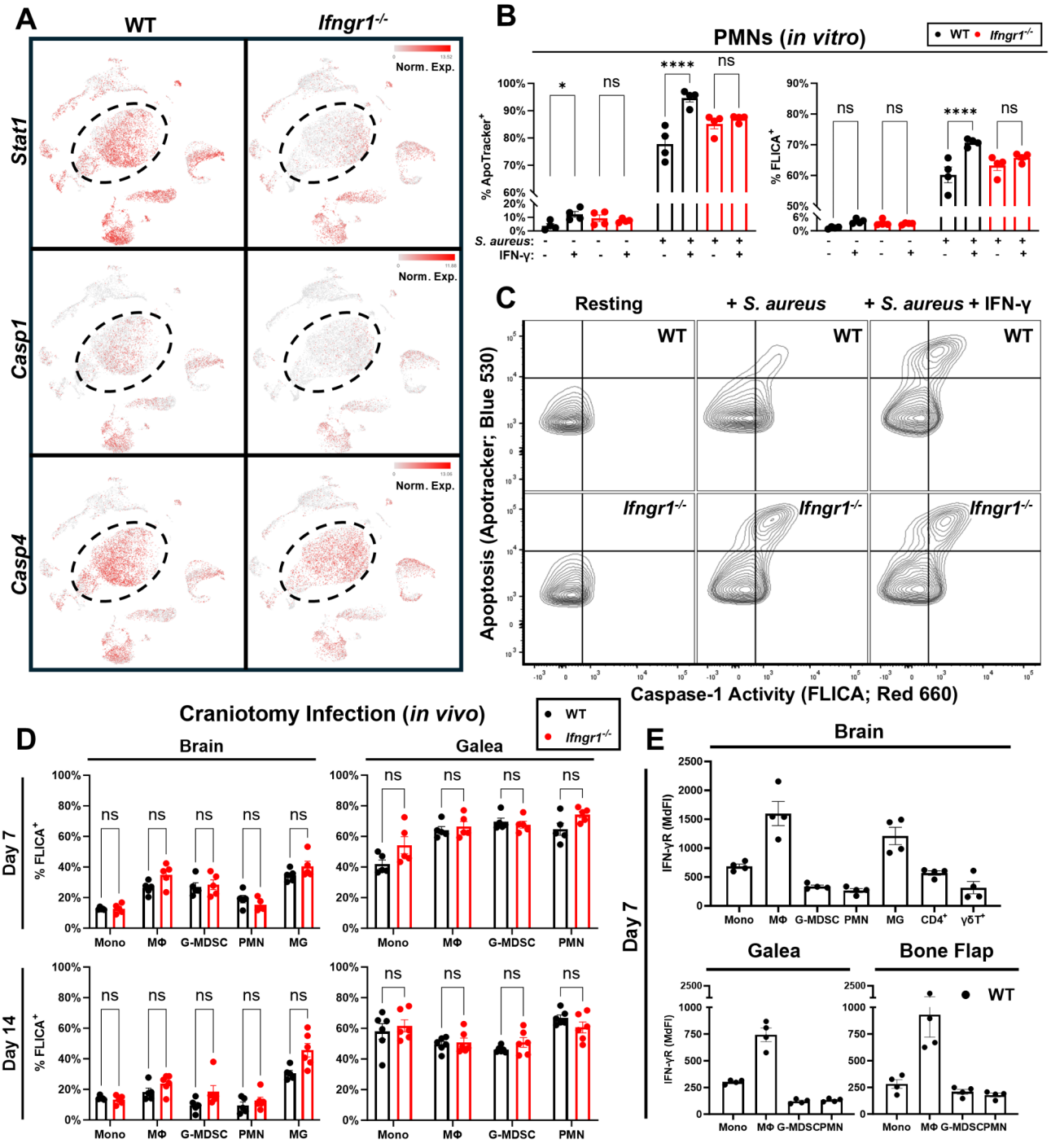

Fig. 4 IFN-γR1 signaling augments neutrophil (PMN) caspase-1 activity. (**A**) Genes associated with pyroptosis are projected on the scRNA-seq UMAP (normalized expression) separated by mouse strain. Dotted circles represent UMAP coordinates of PMN clusters identified in Fig. 2F. (**B**) Primary PMNs from WT and *Ifngr1*$^{-/-}$ mice ($n=4$ biological replicates/group) were pretreated with 200 ng/mL IFN-γ or vehicle for 1 h prior to stimulation with live *S. aureus* at a multiplicity of infection (MOI) of 10:1 (bacteria: PMN) for 1 h, whereupon caspase-1 activity and apoptosis was measured with FLICA and ApoTracker assays, respectively. (**C**) Representative flow plots from (**B**) where unstimulated (- *S. aureus*) + IFN-γ treatment was similar to unstimulated without IFN-γ treatment and is not shown. (**D**) Caspase-1 activity assay in various immune cell populations recovered from the brain and galea at days 7 and 14 post-infection ($n=5$/group). (**E**) IFN-γR1 expression on immune cell populations in WT mice was determined at day 7 post-infection ($n=4$/group). Data representative of (**B**) three or (**D-E**) one independent experiment(s) and were analyzed by (**B**) two-way ANOVA or (**D**) multiple unpaired *t*-test. Mono, monocyte; MΦ, macrophage; ns, not significant; *, $p<0.05$; ****, $p<0.0001$

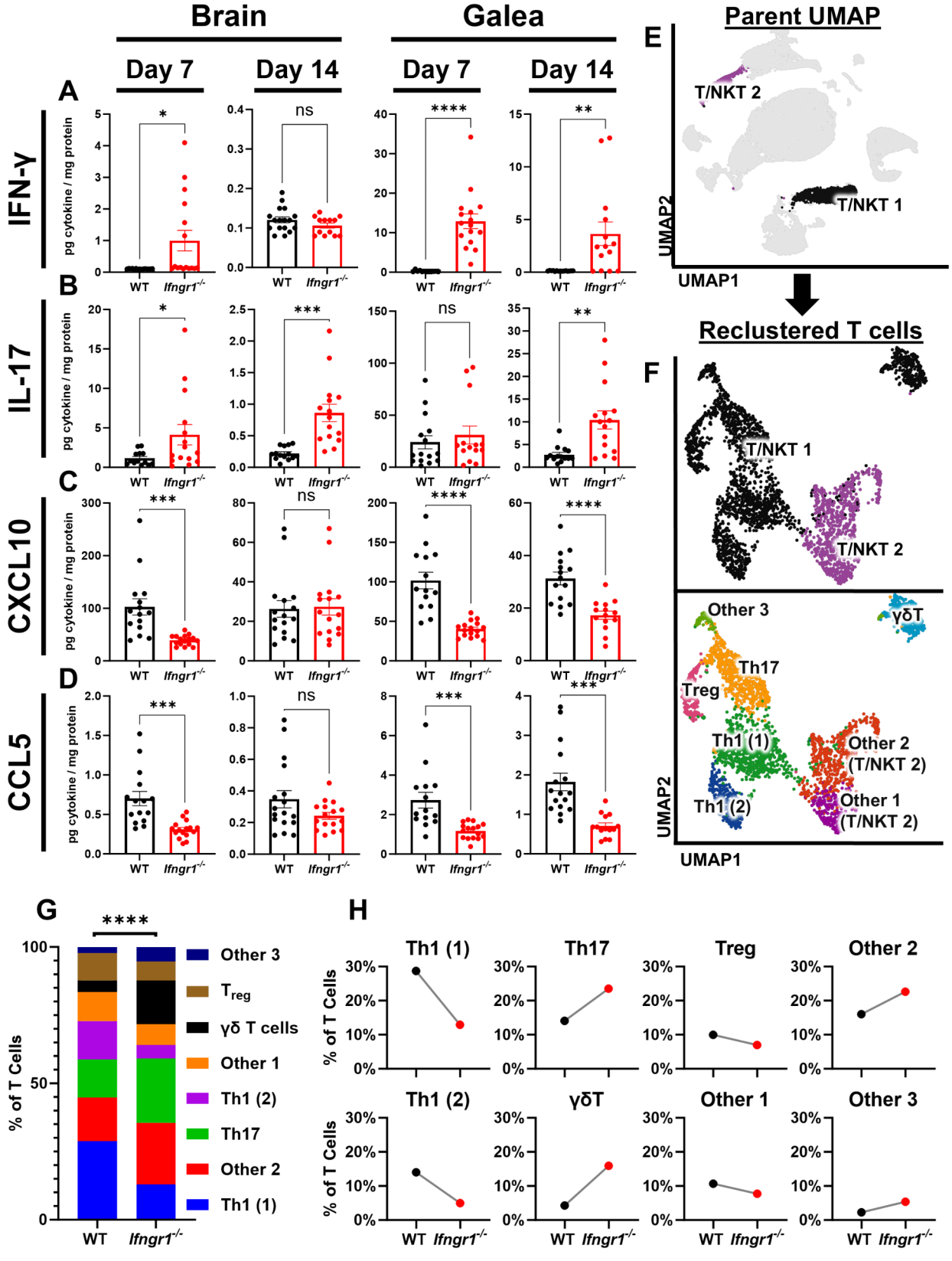

Fig. 5 (See legend on next page.)

(See figure on previous page.)

Fig. 5 *Ifngr1*$^{-/-}$mice display a bias towards CD4^{+} Th17 infiltrates during craniotomy infection. (**A-D**) Inflammatory mediator levels in cell-free homogenates from the brain and galea of WT ($n = 15–17$) and *Ifngr1*$^{-/-}$ ($n = 16$) mice at days 7 and 14 post-infection were assessed by Milliplex multi-analyte bead array. (**E-H**) Analysis of T cell clusters from the scRNA-seq dataset. (**E**) T/NKT cell clusters from the parent UMAP were (**F**) segmented, re-clustered, and annotated. (**G-H**) Comparison of T cell clusters in WT and *Ifngr1*$^{-/-}$ mice. Data analyzed by (**A-D**) two-tailed unpaired *t*-test or (**G**) Chi-square test. ns, not significant; *, $p < 0.05$; **, $p < 0.01$; ***, $p < 0.001$; ****, $p < 0.0001$

infiltrates in the brain at the expense of Th1 cells. We have previously shown that γδ T cells and Tregs do not significantly influence craniotomy infection outcome [27]; therefore, the decreased Th1/Th17 ratio in *Ifngr1*$^{-/-}$ mice is more likely to be biologically relevant.

IFN-γR1 deficiency disrupts T cell-innate immune cell crosstalk

The decreased Th1/Th17 ratio and elevated bacterial burden in *Ifngr1*$^{-/-}$ animals during craniotomy infection is likely mediated by T cell crosstalk with phagocytes since Th cells do not possess direct antibacterial activity and instead exert their effects by activating other immune cells to kill pathogens [77]. To address this possibility, CellChat v2 [54] was employed, a tool capable of inferring cell-cell communication networks from single-cell transcriptomic data. Importantly, this version of CellChat enables comparison of communication networks across samples, where *Ifngr1*$^{-/-}$ and WT mice were evaluated (Additional File 4). Given that most T cells are recruited to the brain (Fig. 2E), the abundance of antigen-presenting cells in the brain vs. galea (Fig. 2B-M), and the previously documented interaction between T cells and macrophages during infection [77], CellChat analysis was restricted to the brain compartment. This revealed unexpected widespread increases in cell-cell interaction count and strength in *Ifngr1*$^{-/-}$ relative to WT samples (Fig. 6A-C), which were attributed to elevated bacterial burden in the former. In contrast, dramatic decreases in T/NKT1 communication with multiple innate immune cell clusters were observed (Fig. 6A-B, Additional File 1: Fig. S8A-B). Reductions in interaction strength and count with T/NKT1 occurred in both incoming and outgoing communication (Additional File 1: Fig. S8B). Importantly, the T/NKT1 cluster is primarily composed of Th cell subsets that exhibited a decreased Th1/Th17 ratio with IFN-γR1 deficiency (Fig. 5F-H). This links decreased Th1 (or increased Th17) representation with inefficient innate immune cell crosstalk, a trend that was particularly strong with monocyte, macrophage, and microglial clusters (Additional File 1: Fig. S8B). Pathway level interrogation of T/NKT1 communication revealed decreases in MHC-I, MHC-II, and CCL (chemokine) signaling in *Ifngr1*$^{-/-}$ mice (Fig. 6D), which was evident across a diverse set of innate immune clusters (Additional File 1: Fig. S9A-C) and corroborated our previous findings (Fig. 5C-D, Additional File 1: Fig. S3A-C). In the absence of IFN-γR1, innate immune clusters instead showed evidence of communication with the non-Th cell cluster T/NKT2 (Fig. 5F) instead of T/NKT1 (Additional File 1: Fig. S9), which may represent an unproductive interaction. IFN-γR1 deficiency was also shown to promote both incoming and outgoing osteopontin (SPP1) signaling in the major macrophage and microglial clusters (Fig. 6E-G). When assessed across all clusters, SPP1 showed widespread communication between multiple nodes in *Ifngr1*$^{-/-}$ mice- a dramatic divergence from WT signaling, which only occurred with a small microglial subset (Microglia 2; Additional File 1: Fig. S9D). Interestingly, SPP1 signaling has been reported to promote Th17 responses by stimulating IL-17 production [78], agreeing with our earlier findings of enhanced Th17 transcriptional signatures (Fig. 5G-H) and IL-17 levels in the brains of *Ifngr1*$^{-/-}$ mice (Fig. 5B). To determine whether Th1 or Th17 cells exert differential effects on macrophage and microglial bactericidal activity, gentamicin protection assays were performed with both populations co-cultured with in vitro polarized Th1 or Th17 cells. While both Th1 and Th17 cells improved macrophage and microglial killing of *S. aureus*, Th1 cells were significantly more effective (Fig. 6H-I), a finding that was IFN-γR1-dependent (Fig. 6J). Collectively, this data suggests a crucial role for IFN-γ signaling in coordinating Th cell crosstalk with macrophages and microglia, likely biasing Th1 infiltrates at the site of craniotomy infection.

Discussion

CD4^{+} T cells are potent modulators of innate immune cell activity [79]. Our recent study established that both Th1 and Th17 cells are important to prevent bacterial outgrowth during *S. aureus* craniotomy infection [27]. However, since both subsets produce multiple cytokines that can impact antibacterial responses, the current study selectively perturbed IFN-γR1 signaling, the major Th1 cytokine, to interrogate its function. *Ifngr1*$^{-/-}$ mice displayed heightened bacterial burdens, which were expected to result from impaired macrophage/microglial activation due to the lack of IFN-γR1 signaling. Surprisingly, *Cx3cr1*^{Cre}*Ifngr1*$^{fl/fl}$ animals displayed no alterations in bacterial growth and few changes in immune cell recruitment relative to *Cx3cr1*^{Null}*Ifngr1*$^{fl/fl}$ WT littermates. Instead, our results implicate a bias towards Th17 responses at the expense of Th1 in the context of global IFN-γR1 deficiency as evident by our scRNA-seq findings of a heightened Th17 transcriptional signature and

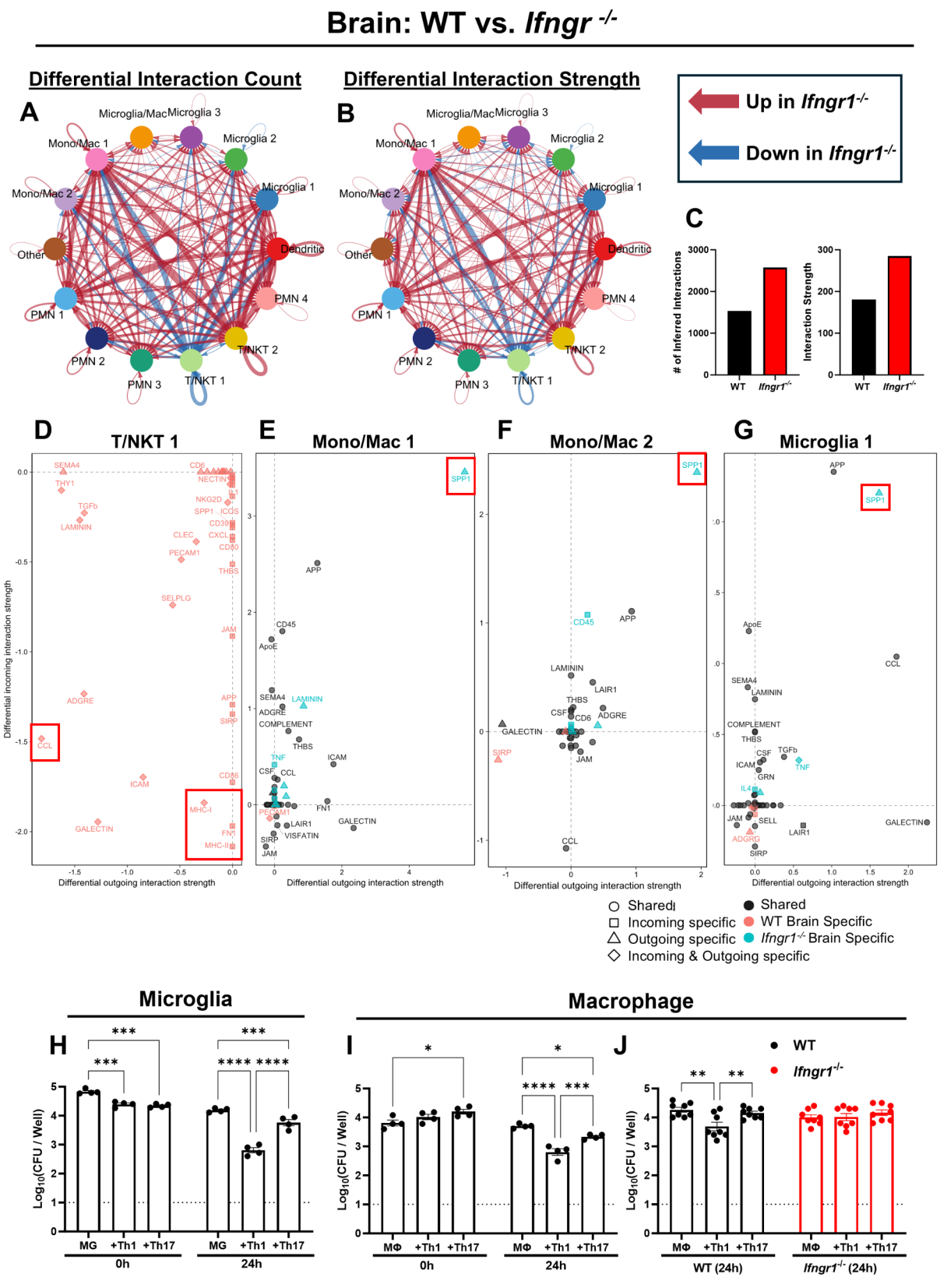

Fig. 6 (See legend on next page.)

(See figure on previous page.)

Fig. 6 Th17 bias in *Ifngr1*$^{-/-}$ mice alters innate-adaptive immune cell crosstalk during *S. aureus* craniotomy infection and antimicrobial activity. (**A-G**) CellChat v2 was used to predict differences in cellular communication across brain clusters between *Ifngr1*$^{-/-}$ and WT mice. Differential predicted interaction (**A**) count and (**B**) strength for *Ifngr1*$^{-/-}$ vs. WT clusters is shown, along with (**C**) quantitative summaries of these metrics for each sample. (**D-G**) Pathway-level differential incoming and outgoing interaction strengths are shown for select clusters. Antibacterial activity of primary (**H**) microglia and (**I-J**) macrophages from WT or *Ifngr1*$^{-/-}$ mice in the presence or absence of Th1 or Th17 CD4$^+$ T cells was assessed by gentamicin protection assay at the indicated timepoints. Data representative of (**H-J**) two independent experiments and analyzed via two-way ANOVA. MG, microglia; MΦ, macrophage; *, $p < 0.05$; **, $p < 0.01$; ***, $p < 0.001$; ****, $p < 0.0001$

elevated IL-17 levels in the brain. The major implications of these results are two-fold.

First, this work suggests that Th1 cells are more efficacious than Th17 cells during *S. aureus* craniotomy infection. Our previous findings were unable to definitively distinguish between the importance of these Th cell subsets since Th17 cells adoptively transferred into *Rag1*$^{-/-}$ mice acquired robust IFN-γ production upon entry to the site of infection and provided similar protection as Th1 cells [27]. In the current report, cellular communication between Th1 and innate immune cells was perturbed with IFN-γR1 loss, which resulted in a reduced Th1/Th17 ratio in the infected brain. This suggests that Th1 cells are more potent at inducing innate immune activation than Th17 cells during craniotomy infection. This is further supported by the lack of increased bacterial burden in TNF-deficient [16] mice, as TNF has been shown to amplify IL-6 signaling that is important for Th17 activation [76, 80]. However, Th17 cells do have some protective function as our data show they can augment macrophage and microglial bactericidal activity, albeit to a lesser extent than Th1 cells. Importantly, both Th1 and Th17 infiltrates are present in infected tissues during human craniotomy infection [2], suggesting that treatments augmenting Th1/Th17 ratios may be effective therapeutic strategies in the future. However, this would need to be carefully regulated to avoid potential concerns about inducing autoimmunity, where autoreactive Th1 and Th17 cells are linked to CNS disorders such as multiple sclerosis [81–83].

Second, since granulocyte- and macrophage/microglia-targeted deletions of *Ifngr1* did not recapitulate the *Ifngr1*$^{-/-}$ phenotype, this suggests that multiple cell types are responsive to IFN-γ that can compensate for the cell-type specific loss of IFN-γR1 to contain infection. An alternative explanation is that Th1 cells stimulate innate immune antimicrobial activity through an IFN-γ-independent mechanism during craniotomy infection. The identification of potential alternate Th1 signals was beyond the scope of the current study; however, our results have identified some candidates. One possible explanation is informed by the reductions in CXCL10 and CCL5 in *Ifngr1*$^{-/-}$ mice, both of which are induced by IFN-γ [74, 75]. Although this did not translate to defects in leukocyte recruitment in *Ifngr1*$^{-/-}$ animals, CXCL10 and CCL5 may activate immune cells already present at the site of infection, which has been described in other pathologies [84, 85]. In addition, CXCL10 can act as an antimicrobial peptide [86], providing another avenue for effects on *S. aureus* growth. Evidence of enhanced SPP1 signaling was also observed in *Ifngr1*$^{-/-}$ mice, suggesting that IFN-γ inhibits SPP1 production, which can have both pro- and anti-inflammatory effects [87, 88]. Interestingly, SPP1 has been linked to HIF1a induction and stabilization as well as Th17 responses which have been shown to be interdependent [78, 89]. We have previously shown that HIF is a key transcriptional regulator of the immune response during craniotomy infection in both mice and humans [2]; therefore, these connections warrant further exploration of the roles of SPP1, CXCL10, and CCL5 in this setting.

Our scRNA-seq data revealed decreased expression of pyroptosis-related genes in *Ifngr1*$^{-/-}$ PMNs during craniotomy infection. In vitro studies confirmed that IFN-γ potentiated caspase-1 activation in PMNs following *S. aureus* exposure; however, this was not observed in *Ifngr1*$^{-/-}$ mice during craniotomy infection. This is likely explained by the fact that numerous other inducers of caspase-1 activity [90, 91], such as IL-1β [15], TNF [16], ROS [14], and bacterial products, are present at the site of infection that likely compensate for the loss of IFN-γ signaling. MHC-II expression was diminished in many innate immune populations in *Ifngr1*$^{-/-}$ mice as detected by scRNA-seq and flow cytometric analysis. This finding was not unexpected, since IFN-γ signaling is recognized as a potent inducer of both MHC-I and MHC-II [38, 92, 93]. Alterations in MHC levels may play an important, and yet uncharacterized, role during craniotomy infection. This would align with our findings of unchecked bacterial growth, where decreased MHC-II in the absence of IFN-γ action would be expected to impair the ability of APCs to present *S. aureus* antigens to T cells, negating an important proinflammatory loop. However, due to the production of superantigens by *S. aureus* capable of activating CD4$^+$ T cells in an antigen-independent manner [2, 94], it remains unclear whether there is a role for antigen-specific T cell activation in this pathology. The topic of T cell antigen specificity during craniotomy infection is an ongoing area of investigation in our laboratory.

This work has several limitations. First, although our findings suggest that a Th17 bias in the absence of IFN-γ signaling may contribute to the failure to contain *S. aureus* replication during craniotomy infection, this was

not directly examined. Additionally, γδ T cells were elevated in our scRNA-seq analysis of *Ifngr1*$^{-/-}$ mice, which was not observed by flow cytometry. This could be due to disparate transcriptional and surface marker expression but remains to be determined. The involvement of alternative factors that could impact bacterial burden (i.e., pyroptosis, MHC-II, SPP1) were not exhaustively explored and remain avenues for future investigation. Cre-Lox genetic systems were used to interrogate cell-type specific contributions of IFN-γ signaling during craniotomy infection. Recombination frequencies using this approach are not absolute and may confound findings; however, identification of decreased MHC-II levels and impaired IFN-γ-dependent responses in microglia and macrophages from *Cx3cr1*^{Cre}*Ifngr1*$^{fl/fl}$ mice make this less likely. It is possible that *S. aureus* superantigens (SAg) are partially responsible for inducing IFN-γ production [95] and the phenotypes in *Ifngr1*$^{-/-}$ mice; however this appears less likely since the USA300 LAC strain used here does not display robust SAg production [96] and the expression of other T cell-derived cytokines during craniotomy infection was not affected. Finally, while identifying Th subsets in mice is relatively straightforward, this is more difficult for human T cells [97] that often present as a mix of multiple subtypes [98–100]. Indeed, we have observed differences in how human T cells impact craniotomy infection using a humanized mouse model [2]. Therefore, findings need to be verified in human cells/tissues where feasible.

In conclusion, we present evidence that IFN-γR1 activity is beneficial during craniotomy infection by augmenting Th cell communication with innate immune cells and favoring Th1 transcriptional responses. Furthermore, Th17 cells elicited suboptimal bacterial killing by macrophages and microglia compared to Th1, providing another example of how IFN-γ effects are dominant. These results highlight the critical role of IFN-γ in the immune response to craniotomy infection.

Abbreviations

CFU	Colony forming units
FACS	Florescence–activated cell sorting
FBS	Fetal bovine serum
G-MDSC	Granulocytic myeloid–derived suppressor cell
GSEA	Gene set enrichment analysis
IPA	Ingenuity pathway analysis
KO	Knock–out
M-CSF	Macrophage colony stimulating factor
PMN	Neutrophil
RBC	Red blood cell
SPP1	Osteopontin
SAg	Superantigen
UMAP	Uniform manifold approximation and projection
WT	Wild type

Supplementary Information

The online version contains supplementary material available at https://doi.org/10.1186/s12974-025-03376-9.

Supplementary Material 1: Additional file 1. Supplementary figures. Document with supplemental figures cited in this manuscript (.pdf). Additional file 2. scRNA-seq sequencing Metrics. Cell Ranger sequencing metrics for samples used in this study (.xlsx). Additional file 3. Cell identification code. Code used to identify cell types at the single-cell level, independent of cluster analysis (.txt). Additional file 4. CellChat v2 code. Code used to impute cellular communication between clusters in our scRNA-seq brain dataset (.txt).

Acknowledgements

The authors thank Dr. Cortney E. Heim for assistance with the scRNA-seq experiment and Dr. Keer Sun for the generous gift of the ***Ifngr1*** conditional knockout mouse strains used in this study.

Author contributions

Conceptualization, G.K. Z.V.R., and T.K.; Methodology, Z.V.R., R.F.; Software, Z.V.R.; Validation, G.K., Z.V.R.; Formal analysis, G.K., Z.V.R.; Investigation G.K., Z.V.R., and C.E.H.; Data curation, Z.V.R.; Writing– original draft preparation, Z.V.R.; Writing–review & editing, G.K. Z.V.R., and T.K.; Visualization, Z.V.R.; Supervision, T.K.; Funding acquisition, T.K.

Funding

This work was supported by the National Institutes of Health/National Institute of Allergy and Infectious Diseases R01 AI169788 (to TK), T32 NS105594, and UNMC Graduate Research Fellowship (to ZVR). The UNMC Genomics Core receives partial support from the National Institute for General Medical Science (NIGMS; INBRE - P20GM103427-19 and COBRE – 1P30GM110768-01). Both the UNMC Genomics and Flow Cytometry Research Cores receive support from The Fred & Pamela Buffett Cancer Center Support Grant (P30CA036727).

Data availability

All scRNA-seq data has been deposited in the GEO database (GSE282637) for public use. All code used for data analysis in this work is provided in Additional Files 3 and 4.

Declarations

Ethics approval

This study was conducted according to the recommendations in the Guide for the Care and Use of Laboratory Animals of the National Institutes of Health and complies with the Animal Research: Reporting of In Vivo Experiments guidelines. The protocol was approved by the University of Nebraska Medical Center Institutional Animal Care and Use Committee (#16-123-10).

Consent for publication

Not applicable.

Competing interests

The authors declare no competing interests.

Received: 3 December 2024 / Accepted: 13 February 2025
Published online: 22 February 2025

References

1. González-Darder JM. Evolution of indications of craniotomy. Trepanation, Trephining and Craniotomy: history and stories. Cham: Springer International Publishing; 2019. pp. 397–405.
2. Van Roy Z, Kak G, Korshoj LE, Menousek JP, Heim CE, Fallet RW et al. Single-cell profiling reveals a conserved role for hypoxia-inducible factor signaling during human craniotomy infection. Cell Reports Medicine. Volume 5, Issue 11, 101790, 2024 https://doi.org/10.1016/j.xcrm.2024.101790
3. Chiang H-Y, Kamath AS, Pottinger JM, Greenlee JDW, Howard MA, Cavanaugh JE, et al. Risk factors and outcomes associated with surgical site infections after craniotomy or craniectomy: clinical article. J Neurosurg JNS. 2014;120(2):509–21.

4. Dashti SR, Baharvahdat H, Spetzler RF, Sauvageau E, Chang SW, Stiefel MF, et al. Operative intracranial infection following craniotomy. Neurosurg Focus. 2008;24(6):E10.
5. Fang C, Zhu T, Zhang P, Xia L, Sun C. Risk factors of neurosurgical site infection after craniotomy: a systematic review and meta-analysis. Am J Infect Control. 2017;45(11):e123–34.
6. Gold C, Kournoutas I, Seaman SC, Greenlee J. Bone flap management strategies for postcraniotomy surgical site infection. Surg Neurol Int. 2021;12:341.
7. Jiménez-Martínez E, Cuervo G, Hornero A, Ciercoles P, Gabarrós A, Cabellos C, et al. Risk factors for surgical site infection after craniotomy: a prospective cohort study. Antimicrob Resist Infect Control. 2019;8:69.
8. Aldrich A, Kuss MA, Duan B, Kielian T. 3D Bioprinted scaffolds containing viable macrophages and antibiotics promote clearance of Staphylococcus aureus Craniotomy-Associated Biofilm infection. ACS Appl Mater Interfaces. 2019;11(13):12298–307.
9. Cheatle J, Aldrich A, Thorell WE, Boska MD, Kielian T. Compartmentalization of immune responses during Staphylococcus aureus cranial bone flap infection. Am J Pathol. 2013;183(2):450–8.
10. Naghavi M, Vollset SE, Ikuta KS, Swetschinski LR, Gray AP, Wool EE, et al. Global burden of bacterial antimicrobial resistance 1990–2021: a systematic analysis with forecasts to 2050. The Lancet. 2024;404(10459):1199– 226.
11. Aldrich AL, Heim CE, Shi W, Fallet RW, Duan B, Kielian T. TLR2 and caspase-1 signaling are critical for bacterial containment but not clearance during craniotomy-associated biofilm infection. J Neuroinflammation. 2020;17(1):114.
12. Aldrich AL, Horn CM, Heim CE, Korshoj LE, Kielian T. Transcriptional diversity and niche-specific distribution of leukocyte populations during Staphylococcus aureus Craniotomy-Associated Biofilm infection. J Immunol. 2021;206(4):751–65.
13. Kak G, Van Roy Z, Heim CE, Fallet RW, Shi W, Roers A, et al. IL-10 production by granulocytes promotes Staphylococcus aureus craniotomy infection. J Neuroinflamm. 2023;20(1):114.
14. Menousek J, Horn CM, Heim CE, Van Roy Z, Korshoj LE, Kielian T. Transcriptional profiling of phagocytic leukocytes and Microglia reveals a critical role for reactive oxygen species in Biofilm Containment during Staphylococcus aureus Craniotomy infection. J Immunol. 2022;209(10):1973–86.
15. Van Roy Z, Arumugam P, Bertrand BP, Shinde DD, Thomas VC, Kielian T. Tissue niche influences immune and metabolic profiles to Staphylococcus aureus biofilm infection. Nat Commun. 2024;15(1):8965.
16. Van Roy Z, Kielian T. Tumor necrosis factor regulates leukocyte recruitment but not bacterial persistence during Staphylococcus aureus craniotomy infection. J Neuroinflamm. 2024;21(1):179.
17. Van Roy Z, Shi W, Kak G, Duan B, Kielian T. Epigenetic regulation of leukocyte inflammatory mediator production dictates Staphylococcus aureus Craniotomy infection outcome. J Immunol. Aug 1;211(3):414-428, 2023.
18. Hegde S, Leader AM, Merad M. MDSC: markers, development, states, and unaddressed complexity. Immunity. 2021;54(5):875–84.
19. Millrud CR, Bergenfelz C, Leandersson K. On the origin of myeloid-derived suppressor cells. Oncotarget. 2017;8(2):3649–65.
20. Veglia F, Sanseviero E, Gabrilovich DI. Myeloid-derived suppressor cells in the era of increasing myeloid cell diversity. Nat Rev Immunol. 2021;21(8):485–98.
21. Medina E, Hartl D. Myeloid-derived suppressor cells in infection: a General Overview. J Innate Immun. 2018;10(5–6):407–13.
22. Ding L, Wan M, Wang D, Cao H, Wang H, Gao P. Myeloid-derived suppressor cells in patients with Acute Pancreatitis with increased inhibitory function. Front Immunol. 2022;13:840620.
23. Loeuillard E, Yang J, Buckarma E, Wang J, Liu Y, Conboy C, et al. Targeting tumor-associated macrophages and granulocytic myeloid-derived suppressor cells augments PD-1 blockade in cholangiocarcinoma. J Clin Investig. 2020;130(10):5380–96.
24. Lv M, Wang K, Huang XJ. Myeloid-derived suppressor cells in hematological malignancies: friends or foes. J Hematol Oncol. 2019;12(1):105.
25. Zhou H, Jiang M, Yuan H, Ni W, Tai G. Dual roles of myeloid–derived suppressor cells induced by toll–like receptor signaling in cancer (review). Oncol Lett. 2021;21(2):149.
26. Zhu DQ, Su C, Li JJ, Li AW, Luv Y, Fan Q. Update on Radiotherapy Changes of Nasopharyngeal Carcinoma Tumor Microenvironment. World J Oncol. 2023;14(5):350–7.
27. Kak G, Van Roy Z, Fallet R, Korshoj LE, Kielian T. CD4 + T cell–innate immune crosstalk is critical during Staphylococcus aureus craniotomy infection. JCI Insight. 2025;10(4):e183327.
28. Ivashkiv LB. IFNγ: signalling, epigenetics and roles in immunity, metabolism, disease and cancer immunotherapy. Nat Rev Immunol. 2018;18(9):545–58.
29. Ellis TN, Beaman BL. Interferon-γ activation of polymorphonuclear neutrophil function. Immunology. 2004;112(1):2–12.
30. Pérez-Figueroa E, Álvarez-Carrasco P, Ortega E, Maldonado-Bernal C. Neutrophils: Many Ways to Die. Frontiers in Immunology. 2021;12.
31. Kato T, Kitagawa S. Regulation of Neutrophil functions by Proinflammatory Cytokines. Int J Hematol. 2006;84(3):205–9.
32. Ma J, Chen T, Mandelin J, Ceponis A, Miller N, Hukkanen M, et al. Regulation of macrophage activation. Cell Mol Life Sci CMLS. 2003;60:2334–46.
33. Trinchieri G, Perussia B. Immune interferon: a pleiotropic lymphokine with multiple effects. Immunol Today. 1985;6(4):131–6.
34. Badie B, Schartner J. Role of microglia in glioma biology. Microsc Res Tech. 2001;54(2):106–13.
35. Rottenberg M, Kristensson K. Effects of interferon-γ on neuronal infections. Viral Immunol. 2002;15(2):247–60.
36. Clemens MJ. Interferons and apoptosis. J Interferon Cytokine Res. 2003;23(6):277–92.
37. Berner V, Liu H, Zhou Q, Alderson KL, Sun K, Weiss JM, et al. IFN-γ mediates CD4 + T-cell loss and impairs secondary antitumor responses after successful initial immunotherapy. Nat Med. 2007;13(3):354–60.
38. Zhou F. Molecular mechanisms of IFN-γ to up-regulate MHC class I antigen processing and presentation. Int Rev Immunol. 2009;28(3–4):239–60.
39. Brutkiewicz RR. Cell signaling pathways that regulate antigen presentation. J Immunol. 2016;197(8):2971–9.
40. Bonville CA, Percopo CM, Dyer KD, Gao J, Prussin C, Foster B, et al. Interferon-gamma coordinates CCL3-mediated neutrophil recruitment in vivo. BMC Immunol. 2009;10:1–13.
41. Jenner RG, Townsend MJ, Jackson I, Sun K, Bouwman RD, Young RA, et al. The transcription factors T-bet and GATA-3 control alternative pathways of T-cell differentiation through a shared set of target genes. Proc Natl Acad Sci U S A. 2009;106(42):17876–81.
42. Hu X, Ivashkiv LB. Cross-regulation of signaling pathways by interferon-gamma: implications for immune responses and autoimmune diseases. Immunity. 2009;31(4):539–50.
43. Verma AK, Bansal S, Bauer C, Muralidharan A, Sun K. Influenza infection induces alveolar macrophage dysfunction and thereby enables noninvasive Streptococcus pneumoniae to cause Deadly Pneumonia. J Immunol. 2020;205(6):1601–7.
44. Verma AK, McKelvey M, Uddin MB, Palani S, Niu M, Bauer C, et al. IFN-γ transforms the transcriptomic landscape and triggers myeloid cell hyperresponsiveness to cause lethal lung injury. Front Immunol. 2022;13:1011132.
45. Blanchette J, Jaramillo M, Olivier M. Signalling events involved in interferon-gamma-inducible macrophage nitric oxide generation. Immunology. 2003;108(4):513–22.
46. Schoenborn JR, Wilson CB. Regulation of interferon-gamma during innate and adaptive immune responses. Adv Immunol. 2007;96:41–101.
47. Liu S, Kielian T. Microglial activation by Citrobacter koseri is mediated by TLR4- and MyD88-dependent pathways. J Immunol. 2009;183(9):5537–47.
48. Thurlow LR, Hanke ML, Fritz T, Angle A, Aldrich A, Williams SH, et al. Staphylococcus aureus biofilms prevent macrophage phagocytosis and attenuate inflammation in vivo. J Immunol. 2011;186(11):6585–96.
49. Sandy-Hodgetts K, Andersen CA, Al-Jalodi O, Serena L, Teimouri C, Serena TE. Uncovering the high prevalence of bacterial burden in surgical site wounds with point-of-care fluorescence imaging. Int Wound J. 2022;19(6):1438–48.
50. Horn CM, Arumugam P, Van Roy Z, Heim CE, Fallet RW, Bertrand BP et al. Granulocytic myeloid-derived suppressor cell activity during biofilm infection is regulated by a glycolysis/HIF1a axis. J Clin Investig. 2024;134(8).
51. Heim CE, Bosch ME, Yamada KJ, Aldrich AL, Chaudhari SS, Klinkebiel D, et al. Lactate production by Staphylococcus aureus biofilm inhibits HDAC11 to reprogramme the host immune response during persistent infection. Nat Microbiol. 2020;5(10):1271–84.
52. Lun ATL, Riesenfeld S, Andrews T, Dao TP, Gomes T, Marioni JC. EmptyDrops: distinguishing cells from empty droplets in droplet-based single-cell RNA sequencing data. Genome Biol. 2019;20(1):63.
53. Alshetaiwi H, Pervolarakis N, McIntyre LL, Ma D, Nguyen Q, Rath JA et al. Defining the emergence of myeloid-derived suppressor cells in breast cancer using single-cell transcriptomics. Sci Immunol. 2020;5(44).
54. Jin S, Plikus MV, Nie Q. CellChat for systematic analysis of cell–cell communication from single-cell transcriptomics. Nat Protoc. 2024.
55. Motulsky HJ, Brown RE. Detecting outliers when fitting data with nonlinear regression - a new method based on robust nonlinear regression and the false discovery rate. BMC Bioinformatics. 2006;7:123.

56. Luckheeram RV, Zhou R, Verma AD, Xia B. CD4 + T cells: differentiation and functions. J Immunol Res. 2012;2012(1):925135.
57. Sallusto F, Lenig D, Mackay CR, Lanzavecchia A. Flexible programs of chemokine receptor expression on human polarized T helper 1 and 2 lymphocytes. J Exp Med. 1998;187(6):875–83.
58. Pesce B, Ribeiro CH, Larrondo M, Ramos V, Soto L, Catalán D et al. TNF-α affects signature cytokines of Th1 and Th17 T cell subsets through Differential actions on TNFR1 and TNFR2. Int J Mol Sci. 2022;23(16).
59. Rothermel CD, Rubin BY, Murray HW. Gamma-interferon is the factor in lymphokine that activates human macrophages to inhibit intracellular Chlamydia psittaci replication. J Immunol. 1983;131(5):2542–4.
60. Casanova JL, MacMicking JD, Nathan CF. Interferon-γ and infectious diseases: lessons and prospects. Science. 2024;384(6693):eadl2016.
61. Pidwill GR, Gibson JF, Cole J, Renshaw SA, Foster SJ. The role of macrophages in Staphylococcus aureus infection. Front Immunol. 2020;11:620339.
62. Gresham HD, Lowrance JH, Caver TE, Wilson BS, Cheung AL, Lindberg FP. Survival of Staphylococcus aureus inside neutrophils contributes to infection. J Immunol. 2000;164(7):3713–22.
63. Schäfer PSL, Dimitrov D, Villablanca EJ, Saez-Rodriguez J. Integrating single-cell multi-omics and prior biological knowledge for a functional characterization of the immune system. Nat Immunol. 2024;25(3):405–17.
64. Aran D, Looney AP, Liu L, Wu E, Fong V, Hsu A, et al. Reference-based analysis of lung single-cell sequencing reveals a transitional profibrotic macrophage. Nat Immunol. 2019;20(2):163–72.
65. Heng TSP, Painter MW, Elpek K, Lukacs-Kornek V, Mauermann N, Turley SJ, et al. The Immunological Genome Project: networks of gene expression in immune cells. Nat Immunol. 2008;9(10):1091–4.
66. Waltman L, van Eck NJ. A smart local moving algorithm for large-scale modularity-based community detection. Eur Phys J B. 2013;86(11):471.
67. Heim CE, West SC, Ali H, Kielian T. Heterogeneity of Ly6G(+) Ly6C(+) myeloid-derived suppressor cell infiltrates during Staphylococcus aureus Biofilm infection. Infect Immun. 2018;86(12):e00684–18.
68. Finak G, McDavid A, Yajima M, Deng J, Gersuk V, Shalek AK, et al. MAST: a flexible statistical framework for assessing transcriptional changes and characterizing heterogeneity in single-cell RNA sequencing data. Genome Biol. 2015;16(1):278.
69. Subramanian A, Tamayo P, Mootha VK, Mukherjee S, Ebert BL, Gillette MA, et al. Gene set enrichment analysis: a knowledge-based approach for interpreting genome-wide expression profiles. Proc Natl Acad Sci U S A. 2005;102(43):15545–50.
70. Krämer A, Green J, Pollard J Jr., Tugendreich S. Causal analysis approaches in Ingenuity Pathway Analysis. Bioinformatics. 2014;30(4):523–30.
71. Rodrigues L, Graça RSF, Carneiro LAM. Integrated Stress Responses to bacterial pathogenesis patterns. Front Immunol. 2018;9:1306.
72. Green DR. Cell Death: Apoptosis and other means to an end. (No Title). 2018.
73. Shlomovitz I, Speir M, Gerlic M. Flipping the dogma - phosphatidylserine in non-apoptotic cell death. Cell Commun Signal. 2019;17(1):139.
74. Liu M, Guo S, Hibbert JM, Jain V, Singh N, Wilson NO, et al. CXCL10/IP-10 in infectious diseases pathogenesis and potential therapeutic implications. Cytokine Growth Factor Rev. 2011;22(3):121–30.
75. Yu X, Song Z, Rao L, Tu Q, Zhou J, Yin Y, et al. Synergistic induction of CCL5, CXCL9 and CXCL10 by IFN-γ and NLRs ligands on human fibroblast-like synoviocytes—A potential immunopathological mechanism for joint inflammation in rheumatoid arthritis. Int Immunopharmacol. 2020;82:106356.
76. Harbour SN, DiToro DF, Witte SJ, Zindl CL, Gao M, Schoeb TR et al. T(H)17 cells require ongoing classic IL-6 receptor signaling to retain transcriptional and functional identity. Sci Immunol. 2020;5(49).
77. Shepherd FR, McLaren JE. T cell immunity to bacterial pathogens: mechanisms of Immune Control and Bacterial Evasion. Int J Mol Sci. 2020;21(17).
78. Murugaiyan G, Mittal A, Weiner HL. Increased osteopontin expression in dendritic cells amplifies IL-17 production by CD4 + T cells in experimental autoimmune encephalomyelitis and in multiple Sclerosis1. J Immunol. 2008;181(11):7480–8.
79. Strutt TM, McKinstry KK, Swain SL. Control of innate immunity by memory CD4 T cells. Adv Exp Med Biol. 2011;780:57–68.
80. Veldhoen M, Hocking RJ, Atkins CJ, Locksley RM, Stockinger B. TGFβ in the context of an inflammatory cytokine Milieu supports De Novo differentiation of IL-17-Producing T cells. Immunity. 2006;24(2):179–89.
81. Dardalhon V, Korn T, Kuchroo VK, Anderson AC. Role of Th1 and Th17 cells in organ-specific autoimmunity. J Autoimmun. 2008;31(3):252–6.
82. Nicholson LB, Kuchroo VK. Manipulation of the Th1/Th2 balance in autoimmune disease. Curr Opin Immunol. 1996;8(6):837–42.
83. Liblau RS, Singer SM, McDevitt HO. Th1 and Th2 CD4 + T cells in the pathogenesis of organ-specific autoimmune diseases. Immunol Today. 1995;16(1):34–8.
84. Pandey V, Fleming-Martinez A, Bastea L, Doeppler HR, Eisenhauer J, Le T et al. CXCL10/CXCR3 signaling contributes to an inflammatory microenvironment and its blockade enhances progression of murine pancreatic precancerous lesions. Elife. 2021;10.
85. Jiao X, Nawab O, Patel T, Kossenkov AV, Halama N, Jaeger D, et al. Recent advances targeting CCR5 for Cancer and its role in Immuno-Oncology. Cancer Res. 2019;79(19):4801–7.
86. Crawford MA, Ward AE, Gray V, Bailer P, Fisher DJ, Kubicka E, et al. Disparate regions of the human chemokine CXCL10 exhibit broad-spectrum antimicrobial activity against Biodefense and antibiotic-resistant bacterial pathogens. ACS Infect Dis. 2023;9(1):122–39.
87. Lin EY, Xi W, Aggarwal N, Shinohara ML. Osteopontin (OPN)/SPP1: from its biochemistry to biological functions in the innate immune system and the central nervous system (CNS). Int Immunol. 2023;35(4):171–80.
88. Zhao Y, Huang Z, Gao L, Ma H, Chang R. Osteopontin/SPP1: a potential mediator between immune cells and vascular calcification. Front Immunol. 2024;15:1395596.
89. Chen L, Yang J, Zhang M, Fu D, Luo H, Yang X. SPP1 exacerbates ARDS via elevating Th17/Treg and M1/M2 ratios through suppression of ubiquitination-dependent HIF-1α degradation. Cytokine. 2023;164:156107.
90. Brokatzky D, Mostowy S. Pyroptosis in host defence against bacterial infection. Dis Model Mech. 2022;15(7).
91. Chai R, Li Y, Shui L, Ni L, Zhang A. The role of pyroptosis in inflammatory diseases. Front Cell Dev Biology. 2023;11.
92. Rosa FM, Fellous M. Regulation of HLA-DR gene by IFN-gamma. Transcriptional and post-transcriptional control. J Immunol. 1988;140(5):1660–4.
93. Giroux M, Schmidt M, Descoteaux A. IFN-gamma-induced MHC class II expression: transactivation of class II transactivator promoter IV by IFN regulatory factor-1 is regulated by protein kinase C-alpha. J Immunol. 2003;171(8):4187–94.
94. Xu SX, McCormick JK. Staphylococcal superantigens in colonization and disease. Front Cell Infect Microbiol. 2012;2:52.
95. Tuffs SW, Goncheva MI, Xu SX, Craig HC, Kasper KJ, Choi J, et al. Superantigens promote < i > Staphylococcus aureus bloodstream infection by eliciting pathogenic interferon-gamma production. Proc Natl Acad Sci. 2022;119(8):e2115987119.
96. King JM, Kulhankova K, Stach CS, Vu BG, Salgado-Pabón W. Phenotypes and virulence among Staphylococcus aureus USA100, USA200, USA300, USA400, and USA600 Clonal lineages. mSphere. 2016;1(3).
97. Mestas J, Hughes CCW. Of mice and not men: differences between Mouse and Human Immunology. J Immunol. 2004;172(5):2731–8.
98. Murphy KM. In search of the CTD. Nat Immunol. 2003;4(7):645.
99. Gor DO, Rose NR, Greenspan NS. TH1-TH2: a procrustean paradigm. Nat Immunol. 2003;4(6):503–5.
100. Allen JE, Maizels RM. Th1-Th2: Reliable paradigm or dangerous dogma? Immunol Today. 1997;18(8):387–92.

Publisher's note